NEOPLASIA
www.neoplasia.com

Volume 12 Number 1 January 2010 pp. 51–60 51

Peritoneal Adhesion and Angiogenesis in Ovarian Carcinoma Are Inversely Regulated by Hyaluronan: The Role of Gonadotropins[1]

Yael Chagit Tzuman*, Stav Sapoznik*, Dorit Granot†, Nava Nevo* and Michal Neeman*

*Department of Biological Regulation, The Weizmann Institute of Science, Rehovot, Israel; †Department of Radiology, Yale University, New Haven, CT, USA

Abstract

Ovarian carcinoma is the leading cause of death among gynecologic cancers. Although transformation of the outer ovarian epithelium was linked with ovulation, the disease is significantly more prevalent and severe in postmenopausal women. We postulated that menopause could augment ovarian cancer progression through the effects of gonadotropins on multifocal seeding to the mesothelial layer lining the peritoneum. This seeding is mediated by integrins as well as by CD44 interaction with hyaluronan (HA). Here, we report the effect of gonadotropins on HA synthesis and degradation and on peritoneal adhesion. A significant concentration- and time-dependent induction in expression levels of *HA synthases* (HASs) and *hyaluronidases* (*Hyals*) was observed *in vitro* on stimulation of human epithelial ovarian carcinoma cells by gonadotropins. Hormonal regulation of HA-mediated adhesion was manifested *in vivo* as well, by fluorescence microscopy of stained MLS multicellular tumor spheroids. The number of spheroids adhered to the mesothelium of ovariectomized CD-1 nude mice 9.5 hours after intraperitoneal insertion was significantly higher than in nonovariectomized mice. Inhibition of HA synthesis by 6-diazo-5-oxo-1-norleucine (DON) both in spheroids and ovariectomized mice significantly reduced the number of adhered spheroids. Thus, the change in the hormonal environment during menopause assists in HA-dependent adherence of ovarian cancer spheroids onto the peritoneum. However, HA is antiangiogenic and it can significantly suppress tumor progression. Accordingly, angiogenesis of the adhered spheroids was significantly elevated in DON-treated tumors. These results can explain the selective pressure that can lead to simultaneously increased tumor expression of both *HASs* and *Hyals*.

Neoplasia (2010) 12, 51–60

Introduction

Throughout menopause, changes in the hormonal milieu could provide important regulatory switches for angiogenesis and tumor progression. These hormonal changes include elevated levels of luteinizing hormone (LH) and follicular-stimulating hormone (FSH) [1] and reduced levels of estrogen and progesterone, which can affect progression of ovarian carcinoma directly and indirectly through their influence on expression of proangiogenic and antiangiogenic factors. Among these changes, the best studied is the effect of the gonadotropin hormones, LH and FSH, which have been shown to be involved in human epithelial ovarian carcinoma. On the one hand, exposure of high hormone levels during menopause or during fertility treatments raised the occurrence of the disease [2–4], and conversely, oral contraceptives, hysterectomy, multiple pregnancies, breast-feeding, and estrogen replacement therapy, which all lessen exposure to gonadotropins, resulted in reduced risk [3,5,6]. Ovarian cancer cells were reported to express receptors for these hormones [7,8] and show a direct response in proliferation rate [9]. Two additional indirect effects have been reported by us. First,

Abbreviations: DON, 6-diazo-5-oxo-1-norleucine; FSH, follicular-stimulating hormone; HA, hyaluronan; HAS, hyaluronan synthase; Hyal, hyaluronidase; LH, luteinizing hormone; VEGF, vascular endothelial growth factor

Address all correspondence to: Michal Neeman, Prof. Department of Biological Regulation, The Weizmann Institute of Science, Rehovot 76100, Israel.
E-mail: michal.neeman@weizmann.ac.il

[1]This work was supported by the US National Institutes of Health grant R01 CA75334, the European Commission 7th Framework ENCITE, and European Research Council Advanced grant 232640-IMAGO. M.N. is incumbent of the Helen and Morris Mauerberger Chair.
Received 26 July 2009; Revised 30 October 2009; Accepted 30 October 2009

DOI 10.1593/neo.91272

elevated expression of *vascular endothelial growth factor* (*VEGF*) [10], which promotes angiogenesis, and second, hormonal-induced expression of integrins and the hyaluronan (HA) receptor CD44 [11], which affects cell adhesion, were induced by LH and FSH. Subsequent studies confirmed elevated expression of VEGF in clinical samples of ovarian carcinomas in addition to dose-dependent VEGF induction by the gonadotropins LH and FSH [12]. These studies suggest that suppression of gonadotropin levels may negatively affect angiogenesis, cell adhesion, and metastasis, resulting in protection from ovarian cancer, yet the role that gonadotropins play in ovarian tumorigenesis remains to be fully elucidated.

An important component of the extracellular matrix (ECM) with respect to ovarian cancer progression is HA [13–15]. HA is a linear, negatively charged, high–molecular weight glycosaminoglycan polymer constructed from repeating [-D-glucoronic acid-β1,3-*N*-acetyl-D-glucosamine-β1,4-]$_n$ units. High–molecular weight HA inhibits angiogenesis during development [16], reproduction [17], and in tumors [18], whereas its products of degradation are known to stimulate endothelial cell proliferation and promote neovascularization [19]. Within the tumor environment, the production of high–molecular weight HA is thought to provide a hydrated matrix which forces gaps in the ECM, facilitating tumor cell migration and metastasis.

Ovarian carcinoma cells often grow as multicellular spheroids in the ascitic fluid. Metastasis in ovarian cancer is initiated by multifocal seeding of cells or small spheroids onto the mesothelial layer lining the peritoneum [20,21]. Those cells recognize and adhere onto HA produced by the mesothelial cells through the HA receptor CD44, in addition to collagen adhesion through the expression of integrins [21]. After collagen binding, the spheroids disintegrate, and HA induces tumor cell motility [13]. Previous studies have revealed a mechanism where rapid HA-mediated attachment is subsequently replaced by stable integrin-mediated contacts [22,23]. In ovarian cancer, the expression of CD44 was linked with better prognosis [24], and yet, as shown previously by us, was induced by gonadotropin stimulation alongside with increased adhesion of the cancer cells onto HA [11].

Ovarian cancer cells manage to overcome the antiangiogenic activity of high–molecular weight HA by the expression of hyaluronidase (Hyal), which degrades HA into proangiogenic fragments. The human and mouse genomes include a family of six *Hyals* that differ in their tissue expression and in the size of fragments they generate [25]. The main *Hyals* studied are *Hyal1* and *Hyal2*. *Hyal1*, which is the most abundant plasma and urine Hyal, is defined by tumor suppressor activity [26] and breaks HA down to small fragments. Hyal2 generates intermediate HA fragments of roughly 20 kDa, which are proangiogenic and are found to have oncogenic activity [25]. Hence, Hyal expression can promote or suppress tumor progression depending on the circumstances of action [27]. Using a self-quenched "smart" magnetic resonance imaging reporter probe, we previously demonstrated the secretion of active Hyal by ovarian carcinoma cells both *in vitro* and *in vivo*, thus allowing the tumor to convert its microenvironment to be proangiogenic [28].

HA is synthesized by a multi-isoform family of transmembrane glycosyltransferases termed the HA synthase (HAS) [29]. Three distinct yet highly conserved eukaryotic HAS isoforms have been identified and termed HAS1, HAS2, and HAS3. HASs were shown to be associated with the progression of various cancers. Recently, it has been shown that HAS1 regulates bladder cancer growth and progression by modulating HA synthesis and HA receptor levels [30]. Elevated *HAS1* expression and/or intronic gene splicing correlates with poor prognosis in human colon cancer, ovarian cancer, and multiple myelomas [31–33]. Expression levels of HA and HAS2, as well as the rate of HA synthesis, were shown to be increased in highly metastatic breast carcinoma cells [34]. Temporary inhibition of HA synthesis in the rat ovary was performed using the metabolic inhibitor DON [17]. Targeted HAS2 suppression in mouse cumulus cell–oocyte complexes was carried out by adenovirus-mediated short-hairpin RNA expression [35].

The goal of this study was to investigate the effect of LH and FSH on HA synthesis and degradation with respect to the peritoneal adhesion and angiogenesis of ovarian carcinoma. We report here that gonadotropins augment the expression of *HAS* and *Hyal in vitro*. Accordingly, elevation of gonadotropin levels *in vivo* by ovariectomy (OVX) enhanced the ability of ovarian carcinoma multicellular spheroids to adhere onto the peritoneum. Inhibition of HA synthesis was sufficient for overcoming the enhanced tumor metastatic implantation induced by OVX. However, angiogenesis was potently suppressed by HA and was significantly augmented by suppression of HA synthesis. Thus, the changes in the hormonal milieu that accompany menopause can lead to increased metastatic implantation of ovarian cancer cells or spheroids on the mesothelial layer lining the peritoneum, whereas degradation of HA was important for tumor angiogenesis and further progression. The hormonal effect on HA metabolism and on the adhesion process, and the impact of HA on tumor angiogenesis, may help shed light on the clinical change in aggressiveness of ovarian cancer in postmenopausal women and further underscore the complexity of HA as a possible target for therapy.

Materials and Methods

Monolayer and Multicellular Spheroid Culture

MLS human epithelial ovarian carcinoma cells were a kind gift from Prof. Robert Sutherland [36]. ES2 cells were kindly provided by Prof. Hauptmann Charite. MLS spheroids were cultured in α-minimum essential medium supplemented with 10% fetal calf serum (Biological Industries, Beit Haemek, Israel), 1% L-glutamine (Biological Industries), and antibiotics: 50 U/ml penicillin (Biological Industries) and 50 μg/ml streptomycin (Biological Industries). Spheroids (0.4-1 mm in diameter) were initiated by plating cells from a confluent culture onto agar-coated plates. Seventy-two hours later, the spheroids were transferred to a 500-ml spinner flask (Belco, Vineland, NJ) at a spinning rate of 80 rpm. The medium was changed every 48 hours for 1 month, and a mixture of 95% air and 5% carbon dioxide was blown over the medium for 5 minutes [37].

Hormonal Stimulation

Human LH and human FSH were a kind gift from Dr. Fortune Kohen. Hormones were dissolved in phosphate-buffered saline and stored at −80°C at a concentration of 1 mg/ml. After 24 hours of culture in serum-free medium, MLS and ES2 human epithelial ovarian carcinoma cell lines were treated with either LH (1 ng/ml) or FSH (1 ng/ml) for varying periods (6, 12, 18, 24, and 48 hours for the MLS cells, and 6, 12, 18, 24, 30, and 36 hours for the ES2 cells).

RNA Extraction, Reverse Transcription, and Polymerase Chain Reaction

After hormonal stimulation, total RNA was isolated from the ovarian carcinoma cell lines using TRI-REAGENT (Molecular Research

Center, Inc., Cincinnati, OH) according to the manufacturer's instructions and was reverse-transcribed in 20-μl (3 μg) volumes using RNase H reverse transcriptase (Super-Script II; Invitrogen Life Technologies, Inc., Carlsbad, CA) with 180 pmol of hexamer random primer. Aliquots (2 μl) of the reverse transcription products were used for polymerase chain reaction (PCR). Semiquantitative PCRs were carried out using primers of interest to determine the transcription level of human HAS1 (NM_001523) (5′-ACTGTACTTTTGGGGATGACC and 5′-CAGCAGAGGGACGTAGTTAG), human HAS2 (NM_005328) (5′-CCCAGCCTCATCTGTGGAG and 5′-ACCCCGGTAGAAGAGCTGG), human HAS3 (NM_005329) (5′-TCGGTGGCACTGTGCATTG and 5′-CTACTTGGGGATCCTCCTG), human Hyal1 (NM_007312.3) (5′-CTATGGCTTCCCTGACTGCT and 5′-GGCAGAAAGTGGTTTGTCGT), and human Hyal2 (NM_033158) (5′-ATGAGTTTGAGTTCGCAGCA and 5′-AGCAGCCGTGTCAGGTAATC). The transcription level of GAPDH (5′-CGGAGTCAACGGATTTGGTCGTAT and 5′-AGCCTTCTCCATGGTGGTGAAGAC) was determined as well and used for calibration of the results. PCR parameters: 2 minutes at 94°C, 5 cycles of 30 seconds at 94°C, 60 seconds at 55°C, 90 seconds at 72°C, followed by 25 cycles (or 19, 21, 23, and 25 cycles for the semiquantitative PCR) of 30 seconds at 4°C, 60 seconds at 60°C, 90 seconds at 72°C, and 10 minutes at 72°C. PCR products were analyzed on agarose gel by measuring their intensity levels.

Animal Protocols

All animal procedures were approved by the Institutional Animal Care and Use Committee.

Ovariectomy. Female CD-1 nude mice (6 weeks old, 20-g body weight) were anesthetized with ketamine HCl (75 μg/g, i.p.) and xylazine HCl (3 μg/g). Both ovaries were removed through 4-mm incisions, and the mice were allowed to fully recover for 2 to 3 weeks.

Spheroid i.p. insertion. One hundred microliters containing approximately 350 fluorescently stained spheroids (0.7 mm in diameter) per mouse were i.p. inserted into OVX CD-1 nude mice. At 5, 7, 9.5, 24, and 96 hours later, mice were killed, equal sizes of peritonea were excised, extensively washed in PBS, and spread out on slides to detect spheroid adhesion by low-resolution fluorescence imaging (IVIS 100; Xenogen, Alameda, CA) and fluorescence microscopy (Axio; Zeiss, Yena, Germany).

Fluorescent Staining of MLS Spheroids

4-Di-10-Asp, a lipophilic tracer, was dissolved in ethanol at 1 mg/ml. Spheroids were washed five times in sterile PBS and then incubated at 37°C with 4-Di-10-Asp (7.5 μg/ml) for 1 hour at 90 rpm. Excess dye was removed by washing the cells with sterile PBS.

Di-D, a lipophilic tracer, was dissolved in ethanol to the concentration of 2 mg/ml. Spheroids were washed five times in sterile PBS and then incubated at 37°C with Di-D (7.5 μg/ml) for 1 hour at 90 rpm. Excess dye was removed by washing the cells with culture medium.

Histology

Peritoneum was fixed in Carnoy solution (ethanol-chloroform-acetic acid, 6:3:1). Histologic sections (5 μm) were stained with hematoxylin and eosin (H&E).

After fixation in 4% paraformaldehyde (PFA), tissues (OVX + DON n = 3, OVX – DON n = 3, non–OVX + DON n = 3, non–OVX – DON n = 3) were embedded in paraffin and sectioned at 4-μm thickness. Sections were deparaffinized for 5 minutes with xylene, ethanol hydrated, antigen retrieved, PBS washed, and blocked in 1% horse serum. Staining was carried out using anti–CD34 antibody (Cedarlane Laboratories, Burlington, NC). Detection of the anti–CD34 antibody was performed by using a biotin-SP–conjugated anti–rat antibody (Jackson ImmunoResearch Laboratories, West Grove, PA) and Cy3-conjugated streptavidin (Jackson ImmunoResearch Laboratories). Staining was detected using a fluorescent microscope (Zeiss Axioscope II; Simple PCI software).

In Situ *Hybridization*

For preparation of HAS2 mRNA probes, RT-PCR was carried out using the following pairs of primers: 5′-GGGCACATCAGGAAGGAAAAC and 5′-ACAGCGTCAAAAGCATGACC. After cloning the fragments using the pGEM-T Easy Vector System (Promega, Madison, WI), digoxigenin-labeled riboprobes were prepared by *in vitro* transcription using the DIG RNA Labeling Kit (Roche, Basel, Switzerland).

Tissues fixed in 4% PFA were embedded in paraffin and serially sectioned at 7-μm thickness (OVX n = 3, non-OVX n = 3). Sections were deparaffinized, hydrated, digested with proteinase K (Sigma Chemical Co., St. Louis, MO), rinsed with TBS, incubated in 4% PFA, dehydrated, and then incubated with a hybridization mixture for 45 minutes at 55°C. Hybridization with the specific probes was carried out overnight at 63°C using 1-μg/ml riboprobes. After the hybridization procedure, sections were washed with SSC, TBS, and then blocked with 1% BSA. For detection of the digoxigenin-labeled riboprobes, sections were incubated with antidigoxigenin alkaline phosphatase (Roche) and stained with NBT/BCIP (Roche). Staining was detected using an E800 microscope and digital camera DXM 1200 (Nikon, Tokyo, Japan).

In Vitro *and* In Vivo *Inhibition of HA Synthesis*

Spheroids were transferred into a 250-ml spinner flask (Belco), and 6-diazo-5-oxo-1-norleucine (DON; Sigma) was added (5 μg/ml) every 24 hours for 2 days. OVX CD-1 nude mice were i.p. injected with DON (7.5-μg/g body weight) every 24 hours for 2 days as well. After 48 hours, 100 μl containing approximately 350 DON-treated spheroids (0.7 mm in diameter) per mouse was stained with 4-Di-10-Asp and i.p. inserted into the DON-treated mice. After spheroid insertion, mice were i.p. injected with DON (7.5 μg/g) once more. At 9.5 hours later, mice were killed, and equal sizes of peritoneum tissues were excised, extensively washed, and spread on slides for further detection of spheroid adhesion by fluorescence imaging and fluorescence microscopy.

Fluorescent Staining of Blood Vessels

Dextran–fluorescein isothiocyanate (FITC; Sigma) or BSA-ROX at the final concentration of 10 mg/ml was i.v. injected (200 μl per mouse) through the tail vein 4 minutes before mouse sacrifice. Equal sizes of peritonea were excised, extensively washed in PBS, and spread out on slides to visualize adhered spheroids and blood vessels by fluorescence microscopy (Axio; Zeiss). Blood vessel density and diameter was analyzed after CD34 staining using Image J (National Institutes of Health; http://rsb.info.nih.gov/ij).

Results

HA Synthesis and Degradation in Ovarian Carcinoma Cells Are Hormonally Regulated

A number of human epithelial ovarian carcinoma cell lines were evaluated for the expression of the *HAS1*, *HAS2*, and *HAS3* genes (Table 1). Whereas none of the cell lines expressed the *HAS1* gene, the MLS and ES2 cell lines were shown to express both *HAS2* and *HAS3*. Because previous studies in our laboratory investigated the expression of VEGF, CD44, and α_V-integrin after LH and FSH stimulation in MLS cells, we therefore selected the MLS cell line for the analysis of *HAS2* and *HAS3* expression levels. MLS cells were treated with either LH or FSH (1 ng/ml) and were analyzed at varying time points (6, 12, 18, 24, and 48 hours). Total RNA was extracted from the cells and reversed-transcribed. Semiquantitative PCR was performed to determine the linear cycle in which *HAS2* and *HAS3* are detected. Induction levels of *HAS2* and *HAS3* were set by PCR of 22 and 23 cycles, respectively. MLS cells stimulated with FSH showed a significant induction in expression levels of both *HAS2* and *HAS3* 24 hours after induction ($n = 4$, $^*P < .05$, two-tailed, equal-variance *t* test; Figure 1*C*). Stimulation with LH caused a significant induction in *HAS2* expression levels 48 hours after induction ($n = 4$, $^*P < .05$, two-tailed, equal-variance *t* test) and in *HAS3* expression levels 24 hours after hormonal treatment ($n = 4$, $^*P < .05$, two-tailed, equal-variance *t* test; Figure 1*D*). To verify that gonadotropins induce HAS expression not only in MLS cells, ES2 cells were treated with either LH or FSH (1 ng/ml) as well and were analyzed at varying time points (6, 12, 18, 24, 30, and 36 hours) for *HAS2* and *HAS3* expression levels. FSH treatment significantly induced *HAS3* expression 6 and 18 hours after induction ($n = 3$, $^*P < .05$, two-tailed, equal-variance *t* test; Figure 1*E*), and LH stimulation significantly induced *HAS3* expression levels 6, 12, and 18 hours after induction ($n = 3$, $^*P < .05$, two-tailed, equal-variance *t* test; Figure 1*F*). The *HAS2* gene was not induced after FSH treatment; nevertheless, enhanced expression was viewed after LH stimulation although not significant.

MLS cells were shown to express the *Hyal1* and *Hyal2* genes as well. Semiquantitative PCR was performed to determine the linear cycle in which *Hyal1* and *Hyal2* are detected. Induction levels of *Hyal1* and *Hyal2* were set by PCR of 24 and 22 cycles, respectively. MLS cells stimulated with FSH demonstrated a significant induction in expression levels of *Hyal1* 6, 24, and 48 hours after induction ($n = 3$, $^*P < .05$, two-tailed, equal-variance *t* test), whereas no significant induction or reduction was detected for *Hyal2* expression levels (Figure 1*G*). MLS cells stimulated with LH exhibited a significant induction in expression levels of both *Hyal1* and *Hyal2* 24 hours after hormonal induction ($n = 3$, $^*P < .05$, two-tailed, equal-variance *t* test; Figure 1*H*).

LH and FSH Elevation Augment Spheroid Adhesion In Vivo

Ovarian cancer metastasis initiates by multifocal seeding of cells or spheroids on the mesothelial layer lining the peritoneum, by binding of cell surface CD44 onto HA produced by the mesothelium [20,21]. Because *HAS2* and *HAS3* expression in the MLS cell line is hormonally regulated *in vitro*, we set out to study the hormonal regulation of HA-mediated adhesion *in vivo*. OVX mice were used here as a model for the hormonal environment associated with ovarian failure during menopause. MLS cells cultured as multicellular tumor spheroids the size of 0.7 mm, and prelabeled with the vital stain 4-Di-10-Asp, were i.p. inserted into OVX CD-1 nude mice ($n = 4$) as well as into non-OVX mice that served as a control ($n = 3$). Mice were killed 5, 7, and 9.5 hours later, and their peritonea were equally excised and extensively washed for spheroid adhesion detection by fluorescence imaging (Figure 2*A*). No ascetic fluid accumulation was observed. Peritoneum tissue from naive non-OVX mice, which was not i.p. inserted with fluorescent spheroids, was added as reference for autofluorescence.

Although the OVX mice displayed increasing signal intensity and spread as the time of adhesion progressed, the non-OVX mice scarcely demonstrated any fluorescence, regardless of the adhesion time (Figure 2*A*) demonstrating a clear differentiation between the peritonea of OVX ($n = 4$) and non-OVX mice ($n = 3$), where adhesion is elevated in the OVX mice. The peritoneum tissues were further visualized by fluorescence microscopy for quantification purposes (Figure 2*B*). The peritoneum in non-OVX mice contained only a small number of adhered spheroids, which were small and on the verge of degradation after 9.5 hours. In OVX mice, the peritoneum contained many adhered spheroids, which were larger and were more intergraded in the tissue as the time progressed (Figure 2*B*). The number of small (≤0.1 mm), large (≥0.1 mm), and bulk aggregates (>1 spheroid) of spheroids was quantified, displaying a significantly greater amount of small, large, and bulks of spheroids detected on the mesothelium of OVX mice compared with non-OVX mice 9.5 hours after insertion ($P < .05$; Figure 2*C*).

Histologic H&E–stained sections showed extensive adherence of spheroids onto the peritoneal tissue of OVX mice 5 hours after insertion (Figure 2*B*). Seven hours after insertion, invasion into the tumor is beginning to develop, and 2.5 hours later, the spheroid had further invaded the tissue (Figure 2*B*). Here, OVX is found to promote the adhesion process by increasing spheroid adhesion and subsequent invasion in the peritoneal cavity.

Tumor and Muscle Expression of HAS2 Is Induced in OVX Mice

MLS cells were cultured as multicellular tumor spheroids, prelabeled with the vital stain 4-Di-10-Asp, i.p. inserted into OVX CD-1 nude mice ($n = 3$) as well as into non-OVX mice that served as a control ($n = 3$) and killed 4 days later. *In situ* hybridization with a HAS2-specific probe was carried out on histologic sections derived from 4-day adhered MLS spheroids in OVX *versus* non-OVX mice. Because both the mouse and human *HAS2* genes are 90% homologues within their coding region, we designed one *HAS2* probe that can detect the *HAS2* gene of both species. The staining indicated an increase in the *HAS2* mRNA levels both in the tumor and in the peritoneal muscle in the OVX group compared with the control (Figure 3). Therefore, OVX induces the expression of *HAS2* mRNA, thus supporting the *in vitro* results seen in Figure 1 where LH and FSH induced the expression of *HAS2*.

Inhibition of HA Synthesis Reduces Spheroid Adhesion In Vivo

The hormonal regulation of HA synthesis on the adhesion process was evaluated *in vivo*. For this purpose, HAS activity was suppressed

Table 1. Expression of HAS by Ovarian Carcinoma Cells.

Cell Line	HAS1	HAS2	HAS3
MLS	–	+	+
OC-238	–	–	–
ES-2	–	+	+
A-27/80	–	–	+
OVCAR	–	–	+

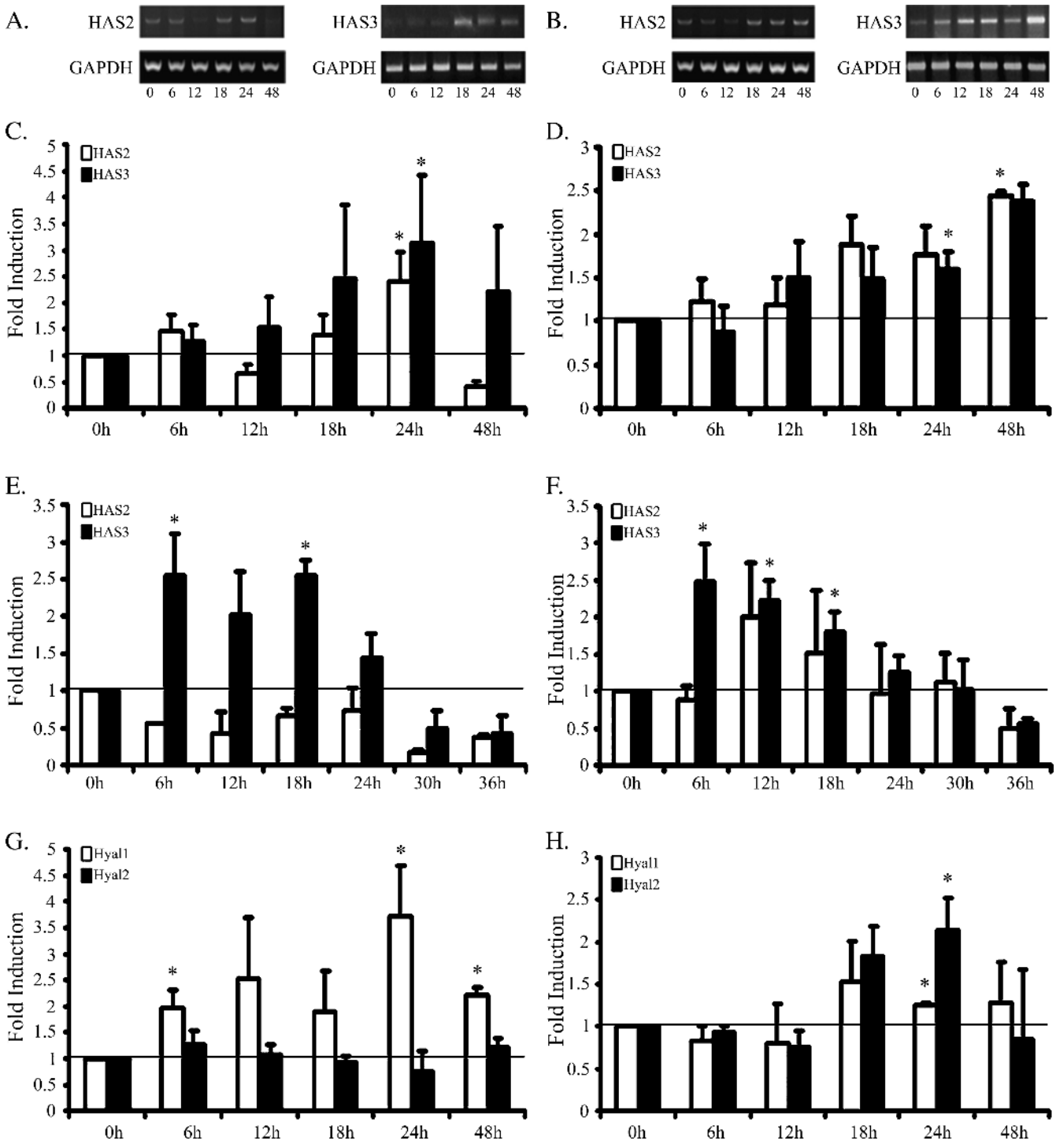

Figure 1. Gonadotropin stimulation regulates HA synthesis and degradation in ovarian carcinoma. MLS and ES2 cells were treated with hLH or hFSH (1 ng/ml) after 6, 12, 18, 24, and 48 hours or after 6, 12, 18, 24, 30, and 36 hours respectively. Cells were harvested, and total RNA was isolated and reverse-transcribed. HAS2, HAS3, Hyal1, and Hyal2 levels were determined by semiquantitative PCR. Band intensity was normalized to GAPDH. (A) Representative agarose gels of *HAS2*, *HAS3*, and *GAPDH* expression in MLS cells after FSH stimulation. (B) Representative agarose gels of *HAS2*, *HAS3*, and *GAPDH* expression in MLS cells after LH stimulation. (C) hFSH's effects on *HAS2* and *HAS3* expression levels at 1 ng/ml in MLS cells (error bars, SE; $*P < .05$, two-tailed, equal-variance *t* test). (D) hLH's effects on *HAS2* and *HAS3* expression levels at 1 ng/ml in MLS cells (error bars, SE; $*P < .05$, two-tailed, equal-variance *t* test). (E) hFSH's effect on *HAS2* and *HAS3* expression levels at 1 ng/ml in ES2 cells (error bars, SE; $*P < .05$, two-tailed, equal-variance *t* test). (F) hLH's effect on *HAS2* and *HAS3* expression levels at 1 ng/ml in ES2 cells (error bars, SE; $*P < .05$, two-tailed, equal-variance *t* test). (G) hFSH's effect on *Hyal1* and *Hyal2* expression levels at 1 ng/ml in MLS cells (error bars, SE; $*P < .05$, two-tailed, equal-variance *t* test). (H) hLH's effect on *Hyal1* and *Hyal2* expression levels at 1 ng/ml in MLS cells (error bars, SE; $*P < .05$, two-tailed, equal-variance *t* test). All *t* tests were compared with time 0.

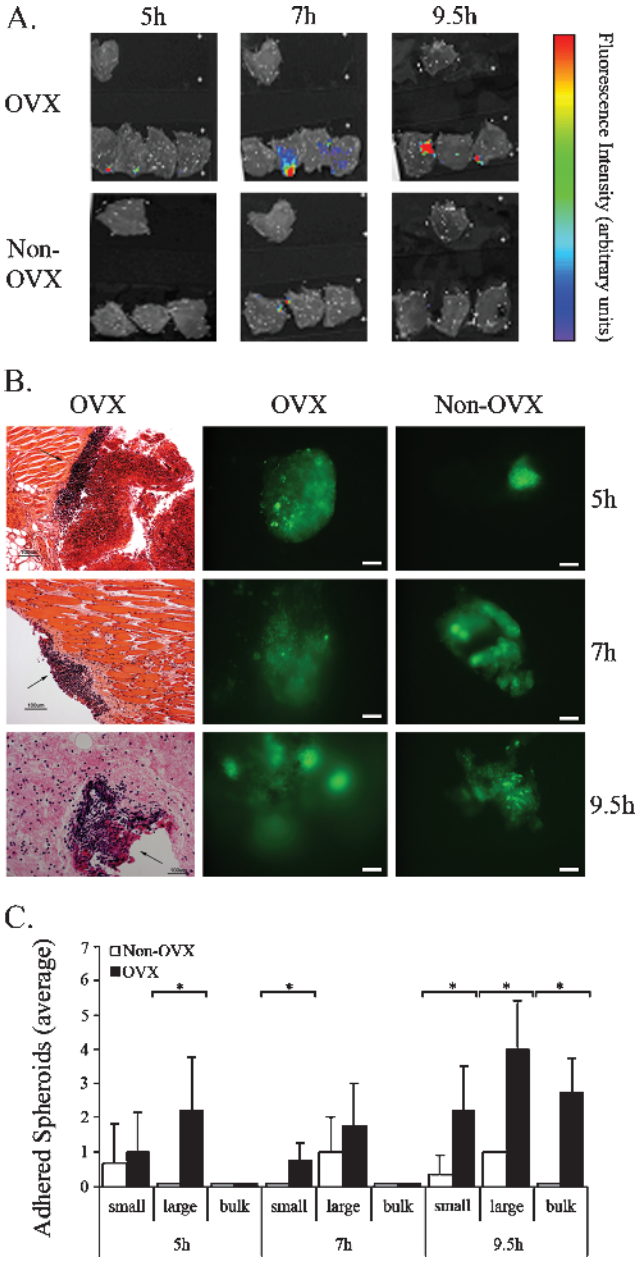

Figure 2. Peritoneal spheroid adhesion is elevated in OVX mice. Spheroids of 0.4 to 0.5 mm were stained with 4-Di-10-Asp and i.p. inserted into CD-1 nude OVX mice. Adhesion was viewed and quantified 5, 7, and 9.5 hours after insertion. (A) Color-coded fluorescent images acquired by the IVIS 100 system of equally excised peritonea (overlaid on a grayscale photograph). The single upper peritoneum in each image represents fluorescence background from a naive mouse. (B) Microscopy of equally excised peritonea. *Left*, H&E staining (*arrows*, adhered spheroid). *Middle and right*, Fluorescent images (*bars*, 0.1 mm). (C) Average number of adhered spheroids measured in equally excised peritonea (OVX, black, $n = 4$; non-OVX, white, $n = 3$). Small, ≤0.1 mm; large, >0.1 mm; bulk, >1 spheroid (error bars, SE; $^*P < .05$, two-tailed, unpaired t test).

both in the spheroids and in the OVX mice by treatment with DON, a metabolic inhibitor of glucosamine synthesis. The average size of DON-treated spheroids (0.32 ± 0.15 mm 2 days after DON treatment) was slightly but significantly larger than spheroids that were not treated with DON (0.23 ± 0.07 mm; data not shown). MLS cells cultured as spheroids (0.7 mm in diameter), and prelabeled with the vital stain 4-Di-10-Asp, were treated with DON and i.p. inserted into CD-1 nude OVX mice treated with DON as well ($n = 5$). Control OVX mice, not treated with DON, were inoculated with nontreated spheroids ($n = 3$). Mice were killed 9.5 hours later, and their peritonea were equally excised and extensively washed to visualize spheroid adhesion by fluorescence imaging and microscopy (Figure 4). No ascetic fluid accumulation was observed. In contrast to the peritoneum of untreated mice showing multiple adhered spheroids, DON-treated spheroids scarcely showed any adhesion, demonstrating the role of HA on the adhesion process (Figure 4*A*). The whole tissue fluorescence microscopy images illustrated a wide spread of fluorescence throughout the DON-treated peritoneum in comparison to the control peritoneum where the fluorescence is very faint and decreased in its spread (Figure 4*A*). The number of small (≤0.1 mm), large (≥0.1 mm), and bulks (>1 spheroid) of spheroids was quantified. On HA synthesis inhibition by DON both in spheroids and OVX mice, the number of large

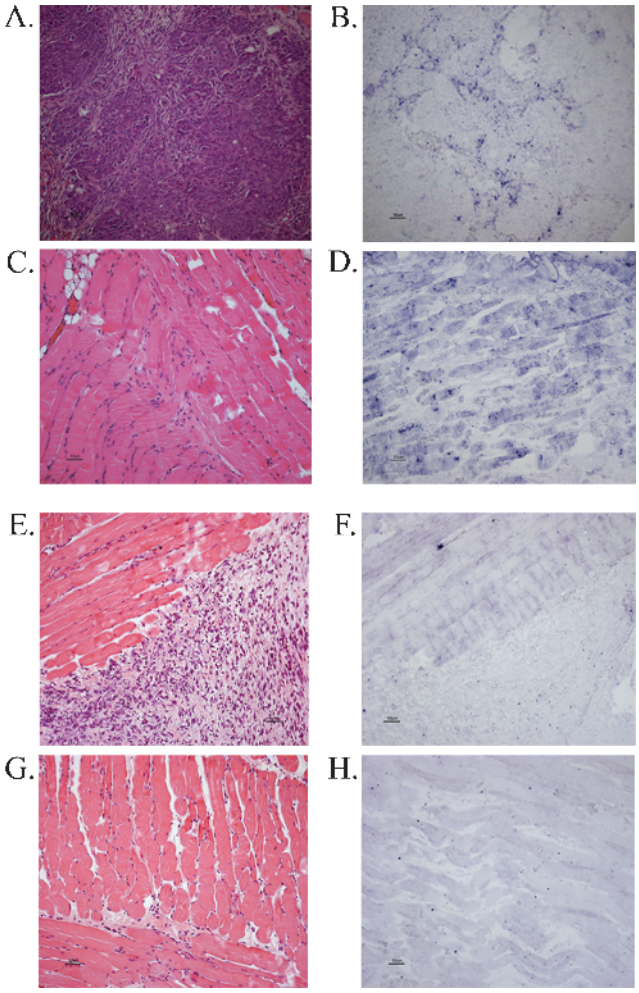

Figure 3. OVX induces HAS2 mRNA levels in the adhered spheroid, and the surrounding muscle. H&E staining and *in situ* hybridization using a HAS2-specific probe on histologic sections of the tumor and the muscle, derived from adhered spheroids 4 days after i.p. insertion into OVX and non-OVX mice. *HAS2* mRNA expression in tumor (A–B) and muscle (C–D) of OVX mice *versus* tumor (E–F) and muscle (G–H) of non-OVX mice (*right panel*, *in situ* hybridization, *left panel*, H&E).

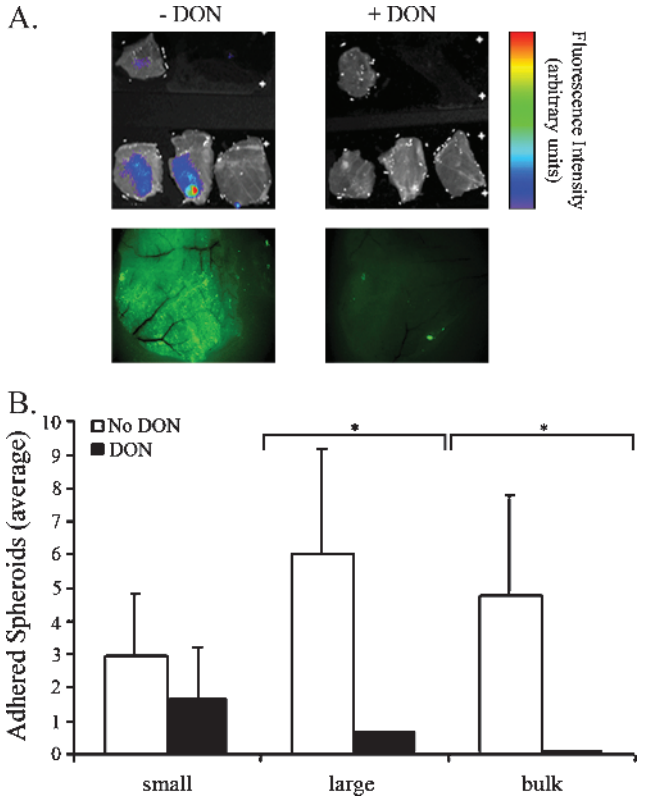

Figure 4. Peritoneal adhesion is mediated by HA. CD-1 nude OVX mice were treated with DON (i.p.; 7.5 μg/g body weight every 24 hours for 2 days). DON was added also to the spheroid culture medium (5 μg/ml every 24 hours for 2 days). Control mice and spheroids were not treated with DON. DON-treated and control spheroids (0.8-1 mm in diameter) were stained with 4-Di-10-Asp and i.p. inserted into DON-treated and control CD-1 nude OVX mice. Adhesion was viewed and quantified 9.5 hours after insertion. (A) *Top*, color-coded fluorescent images of equally excised peritonea (overlaid on a grayscale photograph). The single upper peritoneum in each image represents fluorescence background from a naive mouse. *Bottom*, fluorescent images (Zeiss) of whole peritonea. (B) Average number of adhered spheroids in equally excised peritonea (DON-treated, black, $n = 5$; control, white, $n = 3$). Small, ≤0.1 mm; large, >0.1 mm; bulk, >1 spheroid (error bars, SE; $^*P < .05$, two-tailed, unpaired t test).

and bulks of spheroids detected 9.5 hours after insertion was significantly lower than that in nontreated spheroids and OVX mice ($P < .05$; Figure 4*B*).

Blood Vessel Imaging within the Vicinity of the Tumor

High–molecular weight HA inhibits angiogenesis in normal tissues, in the preovulatory rat follicle [17], and in tumors [18], whereas its degradation products are known to stimulate endothelial cell proliferation and promote neovascularization [19]. We thus aimed to investigate the vasculature in the area of ovarian cancer spheroid adhesion 4 days after insertion. MLS cells were cultured as multicellular tumor spheroids the size of 0.7 mm, which were prelabeled with the vital stain Di-D for spheroid visualization on the peritoneum, and i.p. inserted into two groups of CD-1 nude mice: OVX – DON ($n = 3$), and non–OVX – DON ($n = 3$). Four days later, the mice were i.v. injected with dextran-FITC for blood vessel visualization on the peritoneum 4 minutes before sacrifice. The next two groups of CD-1-nude mice, namely OVX + DON ($n = 3$) and non–OVX + DON ($n = 3$), were i.p. inserted with spheroids prelabeled with 4-Di-10-Asp. Four days later, the mice were i.v. injected with BSA-ROX. Tumors were not yet visible to the naked eye, so equally cut peritonea were washed and removed onto slides for tumor detection by fluorescence microscopy (Figure 5*A*). For quantification purposes of angiogenesis, spheroids the size of 0.7 mm were prelabeled with the vital stain 4-Di-10-Asp and i.p. inserted into four groups of CD-1 nude mice: OVX + DON ($n = 3$), OVX – DON ($n = 3$), non–OVX + DON ($n = 3$), and non–OVX – DON ($n = 3$). Four days later, the mice were i.v. injected with BSA-ROX 4 minutes before sacrifice. Tumor angiogenesis can be visualized in the close surroundings of the tumor 4 days after spheroid inoculation in the untreated groups. Immunohistochemical staining of the spheroid adhesion area using an anti–CD34 antibody revealed enhanced density of blood vessels in the DON-treated groups (Figure 5*B*). Analysis of the average tumor vasculature area percentage (Figure 5*C*), the average number of blood vessels (Figure 5*D*), and the average diameter of blood vessels (Figure 5*E*) revealed significantly increased tumor angiogenesis in DON-treated mice for both OVX and non-OVX, manifested by increased vessel density and area fraction. The diameter of blood vessels seemed to be increased in DON-treated non-OVX mice, but the difference was not statistically significant.

Discussion

HA is an important constituent of the ECM and participates in tumor progression in multiple manners. In ovarian carcinoma, HA is synthesized by HASs expressed by both tumor and stroma cells and participates in tumor cell adhesion. Ovarian carcinoma cells express CD44, the HA receptor, and expression of this receptor was linked with cancer prognosis [34]. Moreover, expression was shown to be regulated by the gonadotropic hormones LH and FSH, thereby providing a mechanism that can explain enhanced metastatic progression in postmenopausal women [13]. HA affects physiological and tumor angiogenesis in a complex manner. High–molecular weight HA can prevent angiogenesis [20], whereas products of its degradation by Hyal are proangiogenic. Remarkably, ovarian cancer cells express and secrete active Hyal [38].

The goal of this study was to evaluate the role of gonadotropin hormones on HA synthesis and degradation and on the metastatic peritoneal adhesion of human epithelial ovarian carcinoma cells. MLS cells treated *in vitro* with either LH or FSH showed significant concentration- and time-dependent induction of *HAS2* and *HAS3* gene expression. The induction pattern suggests that both *HAS2* and *HAS3* genes operate as late-induced genes when stimulated with LH or FSH. Both *HAS2* and *HAS3* stimulated by the LH hormone did not show a decrease in expression levels after the peak because the decrease most probably occurs later than 48 hours after stimulation. *In situ* hybridization in OVX mice indicated an increase in *HAS2* mRNA levels when compared with the staining in non-OVX mice, thus establishing that gonadotropin elevation affects *HAS2* expression.

In vivo, the effects of elevated gonadotropins on mesothelial adhesion were evaluated on OVX mice so as to simulate menopause. The number of MLS spheroids detected on the mesothelium of OVX mice was significantly higher than that in non-OVX mice, suggesting that the change in the hormonal environment due to OVX enhanced the ability of spheroids to adhere onto the peritoneum *in vivo*.

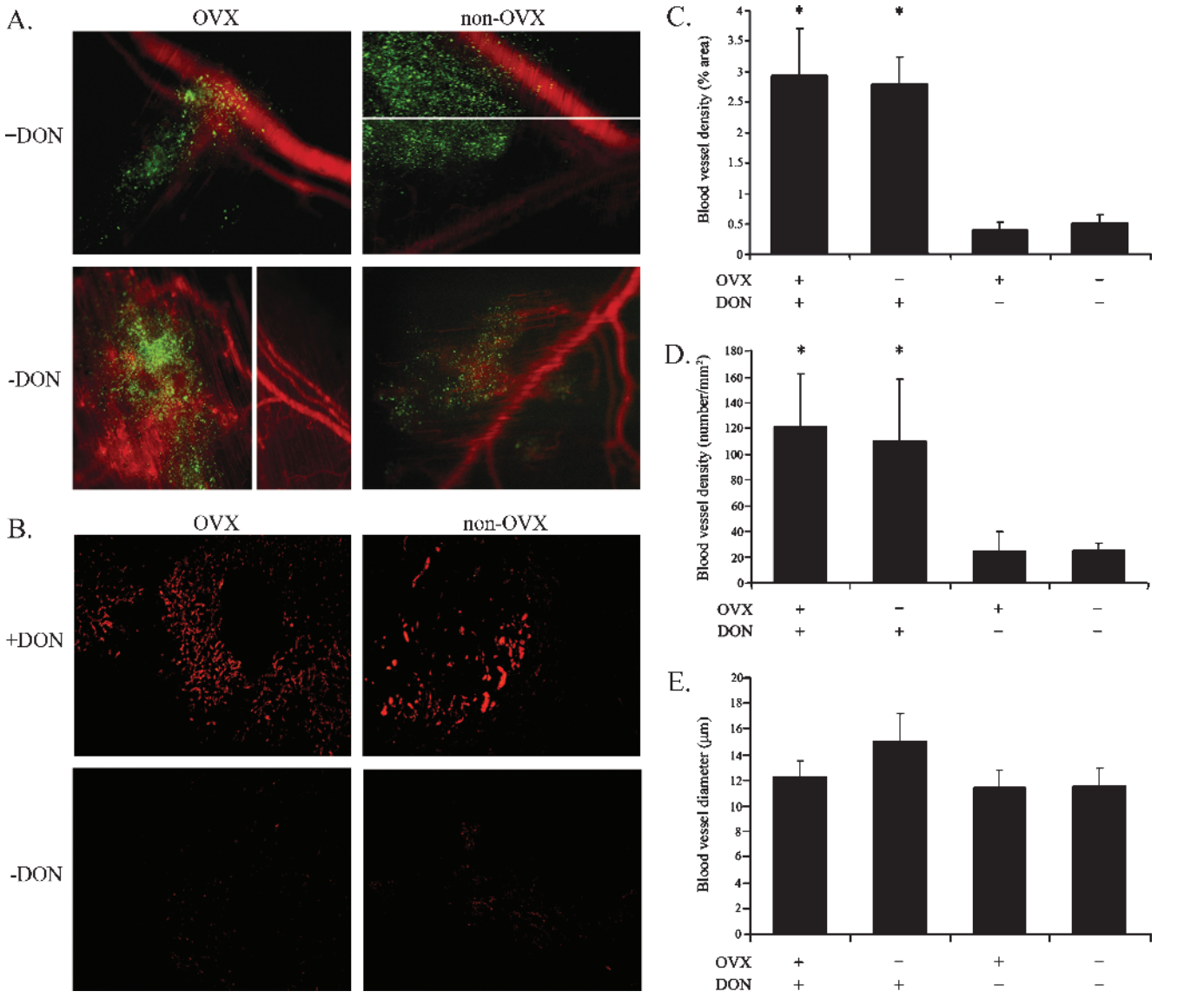

Figure 5. Angiogenesis near adhered spheroids. Spheroids of 0.7 mm were stained with a lipophilic tracer and i.p. inserted into four groups of CD-1 nude mice: OVX + DON, OVX − DON, non–OVX + DON, and non–OVX − DON. Four days later, a macromolecular fluorescent probe was i.v. injected 4 minutes before mice sacrifice. (A) Fluorescent images of adhered spheroids and blood vessels. *Green*, adhered spheroid; *red*, blood vessels. Spheroids from OVX and non-OVX mice treated with DON were stained with 4-Di-10-Asp and i.v. injected with BSA-ROX. Spheroids from OVX and non-OVX mice not treated with DON were stained with Di-D and i.v. injected with dextran-FITC. (B) Immunohistochemical CD34 staining. Spheroids from all four groups were stained with 4-Di-10-Asp and i.v. injected with BSA-ROX. (C) Blood vessel density (area percentage) of tumor vasculature in immunohistochemical CD34 staining slides (error bars, SE; $*P < .05$, two-tailed, unpaired *t* test). (D) Blood vessel density (number/mm^2) in immunohistochemical CD34 staining slides (error bars, SE; $*P < .05$, two-tailed, unpaired *t* test). (E) Average diameter (μm) of blood vessels in immunohistochemical CD34 staining slides.

DON is an effective inhibitor of glucosamine synthesis. It binds to and inactivates the aminotransferase that transfers an amino group from glutamine to fructose-6-P, thus inhibiting the formation of glucosamine-6-P, an intermediate product in the production of UDP-*N*-acetyl glucosamine, a substrate of the HAS enzyme in the process of HA formation [39]. HA synthesis was inhibited both in spheroids and in OVX mice by DON. Consequently, the number of spheroids detected 9.5 hours after insertion was significantly lower than that in nontreated spheroids and OVX mice, confirming that the increased spheroid adhesion in OVX mice *versus* non-OVX mice is due to hormonal regulation on the HAS enzyme. These data imply that inhibition of HAS activity by DON was sufficient for decreasing peritoneal adhesion of ovarian carcinoma spheroids *in vivo*, despite the presence of additional adhesion pathways and despite the DON-treated spheroids being slightly larger than the untreated ones, thus underscoring the contribution of HA synthesis to ovarian carcinoma metastasis.

Peritoneal dissemination of ovarian carcinoma is mediated by CD44-HA dependent adhesion of ovarian cancer cells. We have previously reported that this process is hormonally regulated by exposure to the gonadotropins LH and FSH, which induce the expression of CD44 and increase adhesion of cells onto HA as well [11]. Furthermore,

we have reported that LH and FSH induce the expression of both *VEGF* [3], which promotes angiogenesis, and the α_V-integrin [11], which affects HA-independent tumor adhesion and metastasis. Thus, these current results of the positive gonadotropin affect both HAS levels and the adhesion process and reinforce our hypothesis in which the changes in the hormonal surroundings that accompany menopause may lead to increased implantation of ovarian cancer cells or spheroids on the mesothelial cell layer lining the peritoneal cavity.

HA coating of cells was reported to regulate modular cell adhesion [26]. According to this scheme, HA-coated cells are repelled from HA surfaces, whereas slight HA coating along with the CD44 HA receptor expression will increase adhesion to these surfaces. Accordingly, increased expression of HAS and elevated synthesis of HA by the tumor cells should have reduced peritoneal adhesion, whereas down-regulation of HAS in the tumor cells should increase metastatic spread by exposure of CD44 on the tumor cell surface.

Unexpectedly, LH and FSH treatment elevated *HAS* expression by MLS ovarian carcinoma cells and, despite that, led to an increase in peritoneal spheroid adhesion. Furthermore, adhesion remained HA-dependent and could be suppressed by the inhibition of HA synthesis. Notably, the complexity of HA-regulated adhesion includes not only *HAS* genes that produce a large range of HA molecular sizes but also Hyals expressed and secreted by the tumor cells, which degrade high–molecular weight HA. Here, we show that MLS cells treated *in vitro* with FSH and LH showed a significant concentration- and time-dependent induction of *Hyal1*, whereas *Hyal2* was significantly induced after treatment with LH. The presence of high–molecular weight HA, which inhibits angiogenesis, and the presence of low–molecular weight HA, which promotes angiogenesis, are managed by a balance between the expression of HASs and Hyals, which determine the amount of HA and thus the rate of angiogenesis.

Here, we report that on OVX, the increased levels of LH and FSH cause an induction in *HAS* gene expression, therefore elevating HA levels. HA seems to have a dual activity in the adhesion process. Adhesion occurs on high–molecular weight HA, and once adhered, tumor cells use Hyal to cleave HA into low–molecular weight fragments, thus inducing angiogenesis. As reported here, upon HA synthesis disruption by DON, the angiogenic inhibition by high–molecular weight HA is removed, therefore enabling angiogenesis. Accordingly, anti-CD34 staining was elevated in the DON-treated OVX and non-OVX compared with OVX and non-OVX mice alone. Conversely, functional vessel density in the close vicinity of the adhered spheroids onto the peritonea, detected by intravenously administered dextran-FITC and BSA-ROX, was reduced in DON-treated OVX and non-OVX mice.

Ovarian carcinoma, the most lethal gynecologic malignancy, originates predominantly from the outer epithelium of the ovary [40]. Epidemiological evidence links transformation with ovulation [41]. Thus, interruption of menstruation provides a protective effect independently of whether such interruption was achieved through pregnancy, oral contraceptives, or breast-feeding [42]. Nevertheless, the disease is more prevalent in older patients, and its progress and aggressiveness in relation to other types of cancer is significantly more severe in postmenopausal women. Hence, prolonged tumor dormancy seems to be an integral part of ovarian cancer etiology, where ovarian transformation occurs during ovulation, but the microtumors can remain dormant for a few decades. The hormonal effects reported here on HAS and on adhesion, and the complexity associated with the dual conflicting role of HA on adhesion and angiogenesis, provide further evidence for hormonally regulated changes in the tumor microenvironment, contributing to the increased aggressiveness of ovarian cancer observed during menopause. The clinical impact of this pathway remains to be evaluated.

References

[1] Xu ZR, Wang AH, Wu XP, Zhang H, Sheng ZF, Wu XY, Xie H, Luo XH, and Liao EY (2009). Relationship of age-related concentrations of serum FSH and LH with bone mineral density, prevalence of osteoporosis in native Chinese women. *Clin Chim Acta* **400**, 8–13.

[2] Anderson SM and Dimitrievich E (1996). Ovulation induction for infertility is it safe or not? *S D J Med* **49**, 419–421.

[3] Lacey JV Jr, Mink PJ, Lubin JH, Sherman ME, Troisi R, Hartge P, Schatzkin A, and Schairer C (2002). Menopausal hormone replacement therapy and risk of ovarian cancer. *JAMA* **288**, 334–341.

[4] Rossing MA, Daling JR, Weiss NS, Moore DE, and Self SG (1994). Ovarian tumors in a cohort of infertile women. *N Engl J Med* **331**, 771–776.

[5] Ness RB, Cramer DW, Goodman MT, Kjaer SK, Mallin K, Mosgaard BJ, Purdie DM, Risch HA, Vergona R, and Wu AH (2002). Infertility, fertility drugs, and ovarian cancer: a pooled analysis of case-control studies. *Am J Epidemiol* **155**, 217–224.

[6] Riman T, Dickman PW, Nilsson S, Correia N, Nordlinder H, Magnusson CM, Weiderpass E, and Persson IR (2002). Hormone replacement therapy and the risk of invasive epithelial ovarian cancer in Swedish women. *J Natl Cancer Inst* **94**, 497–504.

[7] Parrott JA, Doraiswamy V, Kim G, Mosher R, and Skinner MK (2001). Expression and actions of both the follicle stimulating hormone receptor and the luteinizing hormone receptor in normal ovarian surface epithelium and ovarian cancer. *Mol Cell Endocrinol* **172**, 213–222.

[8] Syed V, Ulinski G, Mok SC, Yiu GK, and Ho SM (2001). Expression of gonadotropin receptor and growth responses to key reproductive hormones in normal and malignant human ovarian surface epithelial cells. *Cancer Res* **61**, 6768–6776.

[9] Zhou H, Luo MP, Schonthal AH, Pike MC, Stallcup MR, Blumenthal M, Zheng W, and Dubeau L (2002). Effect of reproductive hormones on ovarian epithelial tumors: I. Effect on cell cycle activity. *Cancer Biol Ther* **1**, 300–306.

[10] Schiffenbauer YS, Abramovitch R, Meir G, Nevo N, Holzinger M, Itin A, Keshet E, and Neeman M (1997). Loss of ovarian function promotes angiogenesis in human ovarian carcinoma. *Proc Natl Acad Sci USA* **94**, 13203–13208.

[11] Schiffenbauer YS, Meir G, Maoz M, Even-Ram SC, Bar-Shavit R, and Neeman M (2002). Gonadotropin stimulation of MLS human epithelial ovarian carcinoma cells augments cell adhesion mediated by CD44 and by α(v)-integrin. *Gynecol Oncol* **84**, 296–302.

[12] Wang J, Luo F, Lu JJ, Chen PK, Liu P, and Zheng W (2002). VEGF expression and enhanced production by gonadotropins in ovarian epithelial tumors. *Int J Cancer* **97**, 163–167.

[13] Carpenter PM and Dao AV (2003). The role of hyaluronan in mesothelium-induced motility of ovarian carcinoma cells. *Anticancer Res* **23**, 3985–3990.

[14] Sato E and Yokoo M (2005). Morphological and biochemical dynamics of porcine cumulus–oocyte complexes: role of cumulus expansion in oocyte maturation. *Ital J Anat Embryol* **110**, 205–217.

[15] Tuhkanen H, Anttila M, Kosma VM, Yla-Herttuala S, Heinonen S, Kuronen A, Juhola M, Tammi R, Tammi M, and Mannermaa A (2004). Genetic alterations in the peritumoral stromal cells of malignant and borderline epithelial ovarian tumors as indicated by allelic imbalance on chromosome 3p. *Int J Cancer* **109**, 247–252.

[16] Feinberg RN and Beebe DC (1983). Hyaluronate in vasculogenesis. *Science* **220**, 1177–1179.

[17] Tempel C, Gilead A, and Neeman M (2000). Hyaluronic acid as an anti-angiogenic shield in the preovulatory rat follicle. *Biol Reprod* **63**, 134–140.

[18] Rooney P, Kumar S, Ponting J, and Wang M (1995). The role of hyaluronan in tumour neovascularization [review]. *Int J Cancer* **60**, 632–636.

[19] Slevin M, Krupinski J, Kumar S, and Gaffney J (1998). Angiogenic oligosaccharides of hyaluronan induce protein tyrosine kinase activity in endothelial cells and activate a cytoplasmic signal transduction pathway resulting in proliferation. *Lab Invest* **78**, 987–1003.

[20] Burleson KM, Casey RC, Skubitz KM, Pambuccian SE, Oegema TR Jr, and Skubitz AP (2004). Ovarian carcinoma ascites spheroids adhere to extracellular matrix components and mesothelial cell monolayers. *Gynecol Oncol* **93**, 170–181.

[21] Burleson KM, Hansen LK, and Skubitz AP (2004). Ovarian carcinoma spheroids disaggregate on type I collagen and invade live human mesothelial cell monolayers. *Clin Exp Metastasis* **21**, 685–697.
[22] Cohen M, Joester D, Geiger B, and Addadi L (2004). Spatial and temporal sequence of events in cell adhesion: from molecular recognition to focal adhesion assembly. *Chembiochem* **5**, 1393–1399.
[23] Zimmerman E, Geiger B, and Addadi L (2002). Initial stages of cell-matrix adhesion can be mediated and modulated by cell-surface hyaluronan. *Biophys J* **82**, 1848–1857.
[24] Sillanpaa S, Anttila MA, Voutilainen K, Tammi RH, Tammi MI, Saarikoski SV, and Kosma VM (2003). CD44 expression indicates favorable prognosis in epithelial ovarian cancer. *Clin Cancer Res* **9**, 5318–5324.
[25] Csoka AB, Frost GI, and Stern R (2001). The six hyaluronidase-like genes in the human and mouse genomes. *Matrix Biol* **20**, 499–508.
[26] Wei MH, Latif F, Bader S, Kashuba V, Chen JY, Duh FM, Sekido Y, Lee CC, Geil L, Kuzmin I, et al. (1996). Construction of a 600-kilobase cosmid clone contig and generation of a transcriptional map surrounding the lung cancer tumor suppressor gene (TSG) locus on human chromosome 3p21.3: progress toward the isolation of a lung cancer TSG. *Cancer Res* **56**, 1487–1492.
[27] Stern R (2005). Hyaluronan metabolism: a major paradox in cancer biology. *Pathol Biol (Paris)* **53**, 372–382.
[28] Shiftan L and Neeman M (2006). Kinetic analysis of hyaluronidase activity using a bioactive MRI contrast agent. *Contrast Media Mol Imaging* **1**, 106–112.
[29] Itano N and Kimata K (1996). Molecular cloning of human hyaluronan synthase. *Biochem Biophys Res Commun* **222**, 816–820.
[30] Golshani R, Lopez L, Estrella V, Kramer M, Iida N, and Lokeshwar VB (2008). Hyaluronic acid synthase-1 expression regulates bladder cancer growth, invasion, and angiogenesis through CD44. *Cancer Res* **68**, 483–491.
[31] Yamada Y, Itano N, Narimatsu H, Kudo T, Morozumi K, Hirohashi S, Ochiai A, Ueda M, and Kimata K (2004). Elevated transcript level of hyaluronan synthase 1 gene correlates with poor prognosis of human colon cancer. *Clin Exp Metastasis* **21**, 57–63.
[32] Yabushita H, Noguchi M, Kishida T, Fusano K, Noguchi Y, Itano N, Kimata K, and Noguchi M (2004). Hyaluronan synthase expression in ovarian cancer. *Oncol Rep* **12**, 739–743.
[33] Adamia S, Reiman T, Crainie M, Mant MJ, Belch AR, and Pilarski LM (2005). Intronic splicing of hyaluronan synthase 1 (HAS1): a biologically relevant indicator of poor outcome in multiple myeloma. *Blood* **105**, 4836–4844.
[34] Udabage L, Brownlee GR, Nilsson SK, and Brown TJ (2005). The over-expression of HAS2, Hyal-2 and CD44 is implicated in the invasiveness of breast cancer. *Exp Cell Res* **310**, 205–217.
[35] Sugiura K, Su YQ, and Eppig JJ (2009). Targeted suppression of Has2 mRNA in mouse cumulus cell–oocyte complexes by adenovirus-mediated short-hairpin RNA expression. *Mol Reprod Dev* **76**, 537–547.
[36] Rofstad EK, DeMuth P, Fenton BM, and Sutherland RM (1988). ^{31}P nuclear magnetic resonance spectroscopy studies of tumor energy metabolism and its relationship to intracapillary oxyhemoglobin saturation status and tumor hypoxia. *Cancer Res* **48**, 5440–5446.
[37] Schiffenbauer YS, Tempel C, Abramovitch R, Meir G, and Neeman M (1995). Cyclocreatine accumulation leads to cellular swelling in C6 glioma multicellular spheroids: diffusion and one-dimensional chemical shift nuclear magnetic resonance microscopy. *Cancer Res* **55**, 153–158.
[38] Shiftan L, Israely T, Cohen M, Frydman V, Dafni H, Stern R, and Neeman M (2005). Magnetic resonance imaging visualization of hyaluronidase in ovarian carcinoma. *Cancer Res* **65**, 10316–10323.
[39] Bates CJ, Adams WR, and Handschumacher RE (1966). Control of the formation of uridine diphospho-*N*-acetyl-hexosamine and glycoprotein synthesis in rat liver. *J Biol Chem* **241**, 1705–1712.
[40] Cannistra SA (1993). Cancer of the ovary. *N Engl J Med* **329**, 1550–1559.
[41] Whittemore AS, Harris R, and Itnyre J (1992). Characteristics relating to ovarian cancer risk: collaborative analysis of 12 US case-control studies: II. Invasive epithelial ovarian cancers in white women. Collaborative Ovarian Cancer Group. *Am J Epidemiol* **136**, 1184–1203.
[42] Bose CK (2005). Does hormone replacement therapy prevent epithelial ovarian cancer? *Reprod Biomed Online* **11**, 86–92.